Surface plasmon polariton excitation and manipulation by nanoparticle arrays

V.Coello[a,*] *and S. I. Bozhevolnyi*[b]

[a]Unidad Monterrey CICESE, Alianza Sur 203, Autopista al Aeropuerto Km 10, PIIT CP 66600 Apodaca, NL Mexico.

[b] Institute of Sensors, Signals and Electrotechnics (SENSE), University of Southern Denmark, Niels Bohrs Alle 1E, DK-5230 Odense M, Denmark.

Keywords: Surface plasmons polaritons, Plasmonics, Nanoparticles, Green´s function method
PACS: 73.20.Mf, 71.36.+c, 61.46.Df

Abstract

Using a vectorial dipolar model for multiple surface plasmon-polariton (SPP) scattering [Phys. Rev. B. 67, 165405 (2003)], we investigate the possibility of simultaneous SPP excitation and in-plane manipulation with square-lattice arrays of nanoparticles. The SPP excitation followed by focusing and/or waveguiding of SPP waves is observed with nanoparticle arrays of different shapes, demonstrating the feasibility of the suggested approach.

1. Introduction

In the last years there has been growing interest in the optical manipulation of surface plasmon-polaritons (SPPs) fields. SPPs are electromagnetic excitations coupled to electron plasma oscillations, which have the property of propagating along a metal-dielectric interface as quasi two-dimensional interface waves [1]. SPPs open promising technological perspectives within nano-optics, e.g., for miniaturization of photonics circuits with length scales much smaller than currently achievable, inter-chip and intra-chip applications in computer systems, and bio/sensor-systems [2-4]. SPP micro-optical elements such as mirrors [5-7], band-gap [8] and localization [9] based waveguides, and various focusing structures [10,11] are only some examples of initial attempts to build plasmonic devices. For any plasmonic devices, one has to consider the issue of SPP excitation with free-propagating optical radiation. Traditional SPP excitations methods

* corresponding autor: vcoello@cicese.mx

are based on the use of glass prims as couplers [1]. An alternative is the use of subwavelength hole arrays on a thick metal film as a mechanism for the SPP launching along metal surfaces [12,13]. Another method of SPP excitation consists of optically illuminating a nanostructure (ridge, particle) located at the top of an air/metal interface. Such SPP launching has been used for quantitative experimental analysis of a SPP interferometer [14], SPP focusing with nano-parabolic chains [15], and testing of refractive SPP nano-structures [16].

Considering the SPP interaction with and manipulation by arrays of surface scatterers [5-16], extensive theoretical studies have also been conducted. The theoretical framework, however, is not trivial, since even a relative simple case as the SPP scattering due to a single circular nano-particle requires elaborated numerical simulations [17]. A relative simple scalar multiple scattering approach was used for simulation of SPP micro-components [18] and photonic band gap structures [19] formed by a set of dipolar (nano-sized) scatterers. Here, certain limitations on the accuracy of numerical results should be borne in mind [20]. For example, the effective polarizability of an individual scatterer is a phenomenological quantity that is difficult to relate to scatterer parameters such as size, susceptibility, etc. On the other hand, using the dipole scattering approach a theory for light scattering from a random array of nanoparticles, spaced much less than an optical wavelength, was developed [21]. In this work, the authors deal with the randomness in particle positions by convolving the single-particle Green´s dyadic with a correlation function that describes the average properties of the particle distribution [21]. Furthermore, an approach based on the RLC circuit analogy was developed to produce analytical values for electromagnetic field enhancements within nano-arrays [22]. Lately, the scalar approach of [18] has been extended into a vectorial dipolar model for SPP multiple scattering [20,23] and used to calculate SPP scattering produced by band-gap structures [20] and model the operation of a micro-optical SPP interferometer [24]. Recently, this model was further developed [25] and applied to the problem of SPP guiding by chains of strongly interacting nanoparticles [26]. The developed model is based on the Green´s function formalism and the dipole approximation for field scattering by nanoparticles.

Here, using the vectorial dipolar model for multiple SPP scattering [20,23,25], we investigate the possibility of simultaneous SPP excitation and propagation control with periodic square arrays of nanoparticles illuminated by a normally incident Gaussian beam. SPP focusing and waveguiding are demonstrated with different (in

shape) nano-arrays, exhibiting features that are closely resembled the experimental results for SPP scattering on nanostructures recently reported [15,16]. It should be noted that the light-SPP coupling efficiency in this configuration is expected to be similar to that of a rectangular ridge, since an array of nano-particles in the limit of vanishingly small inter-particle distances should exhibit the scattering properties that are similar to those of a continuous rectangular ridge. Experimental and theoretical investigations of SPP excitation with individual ridges indicated that the overall excitation efficiency for 350-nm-wide and 130-nm-high gold ridges can reach 7% at the free-space wavelength of 800 nm [27]. For our configuration, the direct evaluation of the optimum SPP coupling efficiency using the vectorial dipolar model is cumbersome and typically omitted [28], since it should involve, among other things, a careful analysis of strong particle-surface interactions whose accurate description might require to go beyond the framework of dipole scattering approach [25].

We would like to emphasize that the main idea of the proposed approach is in avoiding the usage (in plasmonic circuits utilizing control of SPP propagation by surface nanostructures) of additional interfacing elements such as, for example, in-coupling ridges and focusing elements.

2. The model

The numerical model is based on the following. When light is incident on a metal/dielectric interface with scattering objects, the objects can be modelled as point-like dipoles. This assumption leads to the construction of an approximate Green´s tensor describing the SPP scattering by such dipoles. The validity of the model is established for relatively large inter-particle distances ($>\lambda_0/2$) whereas for smaller distances one has to include multipolar contributions in the scattered field [20]. Thus, the polarization of the i'th scaterer takes the form:

$$P_i = \alpha \cdot E_0(r_i) + \frac{k_0^2}{\varepsilon_0} \sum \alpha \cdot G(r_i, r_n) \cdot P_n \quad , \tag{1}$$

where α is the polarizability of the scatterers, $E_0(r_i)$ is the incident field at the site of scatterer i, k_0 is the wave vector of the incoming field in the space, $G(r_i, r_n)$ the Green

tensor for SPP to SPP scattering (total field propagator) [20]. The Green tensor is the sum of a direct contribution, $\boldsymbol{G^d}$, in this case the free space Green´s tensor, and an indirect contribution, $\boldsymbol{G^S}$, that describes both reflection from the metal/dielectric interface and excitation of SPPs. Here the polarizability α has the surface dressing included *i.e.* the coupling of the dipole to itself through reflection in the surface. Futhermore, the polarizability, α, is a tensor, describing the polarizability effect in each direction [20]:

$$\alpha = \left(I - k_0^2 \frac{\alpha_0}{\varepsilon_0} \cdot G^S(r,r') \right)^{-1} \cdot \alpha^0 \quad . \tag{2}$$

Where α_0 is the free space polarizability tensor given as

$$\alpha^0 = \varepsilon_0 I 4\pi a^3 \frac{\varepsilon_2 - 1}{\varepsilon_2 + 2} \quad , \tag{3}$$

with I being the unit dyadic tensor. Equation (2) is valid when the long-wavelength electrostastic approximation has been used. Such approximation assumes that the field is constant within the considered range, which corresponds to the size of the scatterer. For the approximation to be valid, the wavelength must be much bigger than the size of the scatterer. If the image dipole approximation is used on $G^S(r,r')$ in Eq. (2) the following result is obtained for the polarizability tensor of Eq. (1).

$$\alpha \approx \left[\frac{\varepsilon_2 - 1}{\varepsilon_2 + 1} \cdot \frac{\varepsilon_2 - 1}{\varepsilon_2 + 2} \left(\frac{1}{8}\hat{x}\hat{x} + \frac{1}{8}\hat{y}\hat{y} + \frac{1}{4}\hat{z}\hat{z} \right) \right]^{-1} \cdot \alpha^0 \quad . \tag{4}$$

It should be mentioned that the dipole approximation assumes that the phase delay of the field, when it moves over the scatterer, is negligible. Mathematically this means $e^{k \cdot r} \cong 1$ for a given field. This means again that the size of the scatterer should be smaller than the wavelength, which is the main assumption in the model. When Eq. (4) has been used in Eq. (1) to determine the polarization, the final step is to calculate the field outside the scatterer as a selfconsistent field:

$$E(r) = E^0(r) + \frac{k_0^2}{\varepsilon_0} \sum_n G(r, r') \cdot P_n \quad . \tag{5}$$

The complete analysis and validity of the model is beyond the scope of this report and can be found elsewhere [20].

3. Numerical results

Following a step-by-step process, first we calculate the in-plane scattered field created by a normally incident Gaussian beam (λ_0=750 nm, FWHM=5μm, *x*-pol) of unit amplitude impinging on a 150-nm-period square lattice (width $w \approx 1.05$ μm, length $L \approx$ 15μm) of nanoparticles with radius, *r*, of 20 nm (Fig. 1(a,b)). The entire system is simulated on a gold surface with dielectric constant ε=-23.11+1.4i. The configuration and the illumination conditions, in general, can be considered as fairly similar to experimental realized ones [15, 16], for example, the wavelength of 750 nm can be experimentally obtained by using a wavelength-tunable (700-860nm) Ti:sapphire laser. Fig. 1(b) shows numerical simulations of a direct SPP excitation taking place at the lower (along y-axis) nanoarray edge. Hereafter, for all images, the total field is calculated 80 nm above the air-gold interface, and the incident beam has been removed; i.e; only scattered SPP appear in the pictures. Fig. 1(c) shows the power of the SPP beam propagating in the positive direction of *y*-axis calculated as a function of the incident beam position (along the *y*-axis). The calculations were made for two distinct *w* values. An asymmetric behavior was exhibited in both calculated curves. One can notice that once the incident beam is not in contact with the nanoarray, the optical power is weak (Fig. 1(c)); this is expected, considering that no SPP can be launched without interacting with the nanoarray. Once the launching of SPP is achieved, in this way, from an application point of view, one can exploit the nanoarrays in order to manipulate the SPP propagation.

A nanodevice, realizable by a certain array structure, is a focusing micromirror. The concept is to place nanoparticles along a parabolic chain $(y - y_0) = 4F(x - x_0)^2$ where the coordinate (x_0, y_0) is located at the bottom of the mirror which coincides with

the incident beam position, the *y* axis is oriented along the optical axis and *F* is the focal length. (Fig. 2 (a), (b)). A nanodevice, realizable by a certain array structure, is a focusing micromirror. The concept is to place nanoparticles along a parabolic chain $(y-y_0)=4F(x-x_0)^2$ where the coordinate (x_0,y_0) is located at the bottom of the mirror which coincides with the incident beam position, the *y* axis is oriented along the optical axis and *F* is the focal length. (Fig. 2 (a), (b)). We simulated nanomirrors with *F*= 4 μm (Fig. 2(a)) and *F*= 8 μm (Fig. 2(b)). In both cases, the focusing effect was clearly seen. For applications matters, focusing nano-mirrors give the possibility to enhance SPP signal locally in a controllable way. Thus, if the maximum intensity at the focal point is several orders of magnitude bigger than the one of the incident beam, one can think to exploit such mirrors in, for example, bio sensors, and surface enhanced Raman spectroscopy. In this context, it has been found that the focusing efficiency strongly depend on the mirror curvature radius, *R*, and the size of the illumination spot, *W* [28]. Strong SPP focusing effects have been reported for relatively larger *W*☜*R*. Moreover, in analogy with SPP focusing by circular slits [29], for an optimization of the SPP focusing efficiency, the parabolic mirror radius, the SPP propagation length, and the incident beam width should be of similar values [28].

Scattering of the plasmons at nanoparticle arrays also enables guiding of the SPPs. A particularly simple geometry of a plasmon waveguide is presented in Fig. 3(a-d). The waveguide consists of a periodic square-shaped nanoarray of $w \approx 2\mu m$, and $L \approx 15\ \mu m$. We launched plasmons by illuminating, with a normally incident Gaussian beam (λ_0=750 nm, FWHM=2.5 μm, *y*-pol), either end of the nanoarray. The SPP waveguiding capability is evidenced by the SPP beam coming out of the waveguide (Fig. 3(a,b)). In contrast, SPP waveguiding is almost not observed when the incident beam is placed on the midsection of the nanoarray (Fig. 3(c)). At the midsection, the nanoarray is almost symmetric over the extent of the incident beam and therefore cannot scatter efficiently in the axial direction since the incoming propagating vector and the propagating SPP vector are hardly matched. However, this symmetry is broken at the nanoarrays ends where light is scattered into propagating SPP modes. Likewise, propagating SPP modes are excited in thin-film surface utilizing gratings or dots. Optical power is slightly decreased as the incident beam is in less contact with the left entrance position of the nanoarray (Fig. 3(d)) thus bringing a less efficiency in the SPP launching and guiding. In analogy with light propagation in optical fibres, SPP propagation is not limited to

symmetric-straight nanostructures. For example, a square-shaped nanoarray with tapered exit (right end) can be proved for SPP focusing (Fig. 4(a)). The effect is better seen, in the outcome SPP, when the exit of the nanoarray is a semi-circumference (Fig. 4(b)).

3. Conclusions

Summarizing, we modeled SPP excitation and manipulation by nanoarrays whose main elements represent individual nanoparticles lined up and equally spaced. The feasibility of simultaneous excitation, propagation and manipulation of SPP fields was corroborated. The numerical calculations were carried out by using a relatively simple vectorial dipolar model for multiple SPP scattering [20] that allows one to explicitly formulate the set of linear equations for the self-consistent field, facilitating greatly computer-aided design considerations. The SPP launching was simulated elucidating the influence of square-shaped nanoarray width. Focusing and waveguiding of SPP were studied by using several system parameters as different focal lengths and incident beam positions. The functionality of non-symmetric nanoarrays, with guiding and focusing properties, was also corroborated. The results show the feasibility to manipulate SPPs without using external excitation elements as for example a in-coupling ridge. In order to explore more this possibility further theoretical and experimental works are needed.

Acknowledgements.

One of us (V.C.) acknowledges financial support from CONACyT project SEP-2004-C01-45999.

References

[1] H. Raether, Surface Plasmons, Springer Tracts in Modern Physics Vol. 111 (Springer, Berlin, 1988), V. M. Agranovich and D. L. Mills (eds.), Surface Polaritons (North-Holland, Amsterdam, 1982).

[2] R. Zia, J. A. Schuller, and M. L. Brongersma, Maters.Today **9**, 20 (2006).

[3] W.L. Barnes, A. Dereux, and T.W. Ebbesen, Nature **424**, 824 (2003).

[4] T.W. Ebbesen, C. Genet and S.I. Bozhevolnyi, Physics Today, **61** (5), 44 (2008).

[5] I. I. Smolyaninov, D. L. Mazzoni, and C. C. Davis, Phys. Rev. Lett. **77**, 3877 (1996).

[6] S.I. Bozhevolnyi and F. Pudonin, Phys. Rev. Lett. **78**, 2823 (1997).

[7] I. I. Smolyaninov, D. L. Mazzoni, J. Mait, and C. C. Davis, Phys. Rev. B **56**, 1601 (1997).

[8] S. I. Bozhevolnyi, J. Erland, K. Leosson, P. M. W. Skovgaard, and J. M. Hvam, Phys. Rev. Lett. **86**, 3008 (2001).

[9] S. I. Bozhevolnyi, V. S. Volkov, and K. Leosson, Phys. Rev. Lett. **89**, 186801 (2002).

[10] Z. Liu, J.M. Steele, W. Srituravanich, Y. Pikus, C. Sun, X. Zhang, Nano Lett. **5,** 1726 (2005).

[11] A. Drezet, A.L. Stepanov, H. Ditlbacher, A. Hohenau, B. Steinberger, F.R. Aussenegg, A. Leitner, J.R. Krenn, Appl. Phys. Lett. **86,** 074104 (2005).

[12] D. S. Kim, S. C. Hohng, V. Malyarchuk, Y. C. Yoon, Y. H. Ahn, K. J. Yee, J.W. Park, J. Kim, Q. H. Park, and C. Lienau, Phys. Rev. Lett. **91**, 143901 (2003).

[13] E. Devaux, T. W. Ebbesen, J.-C. Weeber and A. Dereux, Appl. Phys. Lett. **83**, 4936 (2003).

[14] A. Drezet, A. Hohenau, A. L. Stepanov, H. Ditlbacher, B. Steinberger, F. Aussenegg, A. Leitner, J. Krenn, Plasmonics **1,** 141 (2006)

[15] I. P. Radko, S. I. Bozhevolnyi, A. B. Evlyukhin, and A. Boltasseva, Optics Express, **15**, 6576 (2008).

[16] I. P. Radko, A. B. Evlyukhin, A.Boltasseva, and S. I. Bozhevolnyi, Optics Express, **16**, 3924 (2008).

[17] A. V. Shchegrov, I. V. Novikov, and A. A. Maradudin, Phys. Rev. Lett. **78**, 4269 (1997).

[18] S.I. Bozhevolnyi and V. Coello, Phys. Rev. B **58**, 10899 (1998).

[19] S.I. Bozhevolnyi and V.S. Volkov, Opt. Commun. **198**, 241 (2001).

[20] T. Søndergaard and S. I. Bozhevolnyi, Phys. Rev. B **67**, 165405 (2003).

[21] B. J. Soller and D. G. Hall, JOSA B, **19**, 2437 (2002).

[22] D. A. Genov, A. K. Sarychev, V. M. Shalaev, and A. Wei, Nano Lett. **4**, 153 (2004).

[23] T. Søndergaard and S. I. Bozhevolnyi, Phys. Rev. B **69**, 045422 (2004).

[24] V. Coello, T. Søndergaard, and S.I. Bozhevolnyi, Opt. Comm. **240,** 345 (2004).

[25] A. B. Evlyukhin and S. I. Bozhevolnyi, Phys. Rev. B **71**, 134304 (2005).

[26] A.B. Evlyukhin and S.I. Bozhevolnyi, Laser Phys. Lett. **3,** 396 (2006).

[27] I. P. Radko, S. I. Bozhevolnyi, G. Brucoli, L. Martín-Moreno, F. J. García-Vidal, and A. Boltasseva, Phys. Rev. B **78**, 115115 (2008).

[28] A. B. Evlyukhin, S. I. Bozhevolnyi, A. L. Stepanov, R. Kiyan, C. Reinhardt, S. Passinger, and B. N. Chichkov, Optics Express, **15**, 16667 (2007).

[29] Z. Liu, J. M. Steele, W. Srituravanich, Y. Pikus, C. Sun, and X. Zhang, Nano Lett. **5**, 1726 (2005).

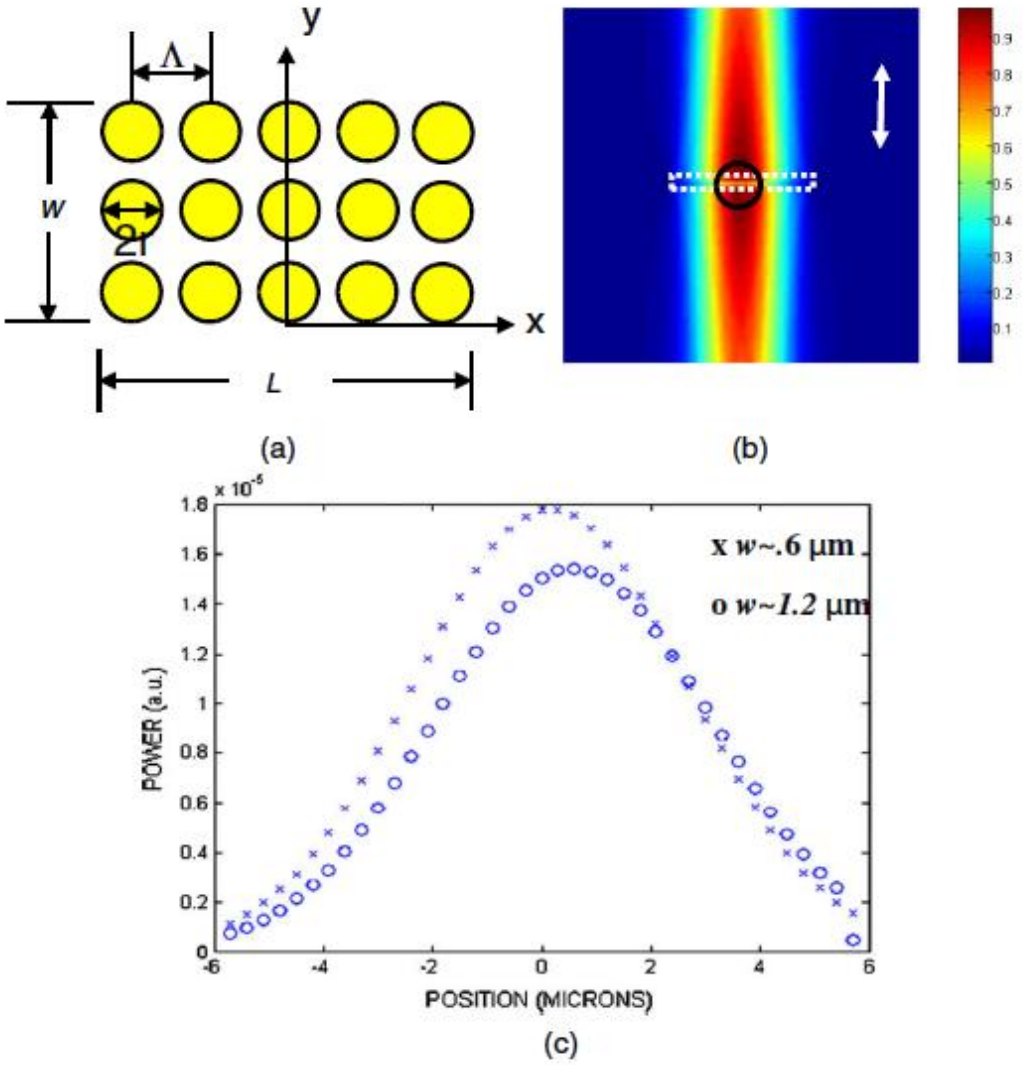

Fig. 1. (a) Schematic layout of a periodic square-lattice gold nanoparticle array, where *r* is the particle radius, *L*, *w*, and *Λ* are the array length, width, and period, respectively. (b) Electric field magnitude distribution (40x40 μm^2) calculated at the height of 80 nm above the air-gold interface for the incident (solid circle) Gaussian light beam (wavelength, λ=750 nm, FWHM=5μm, the polarization is along *y* axis) being incident on the nanoarray (dotted square). The lateral size of the nano-array is 150 nm. (c) The power of the SPP beam propagating in the positive direction of *y*-axis calculated as a function of the incident beam position (along the *y*-axis) for two array width *w* values. The arrow in (b) indicates the incident light polarization.

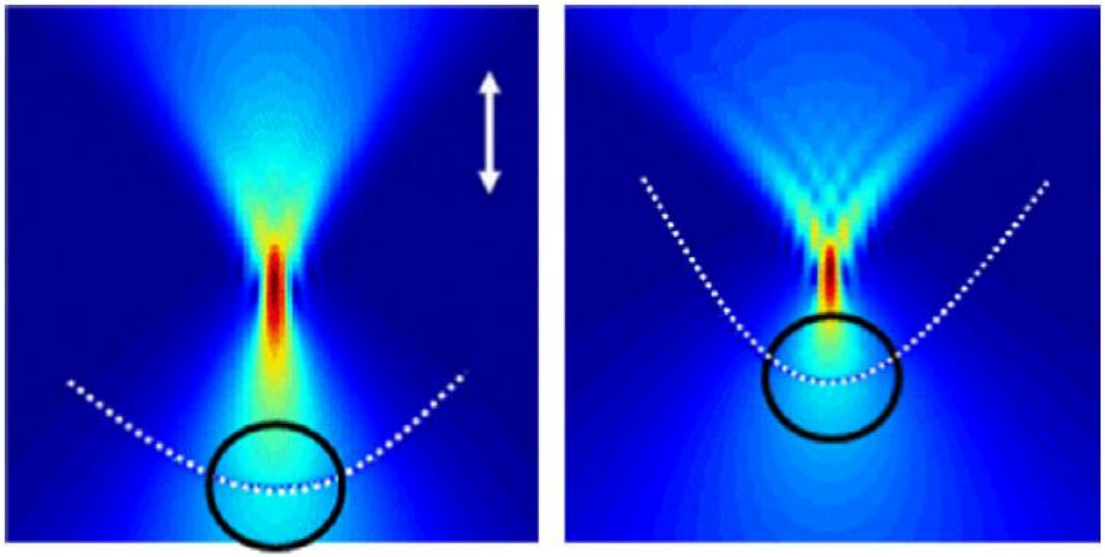

Fig. 2. Electric field magnitude distributions calculated for curved nanomirrors with *F* (a) =4 μm and (b) 8 μm. The dotted line represents the curved nanomirror. The arrow indicates the incident light polarization in both cases. All else is as in Figure 1(b).

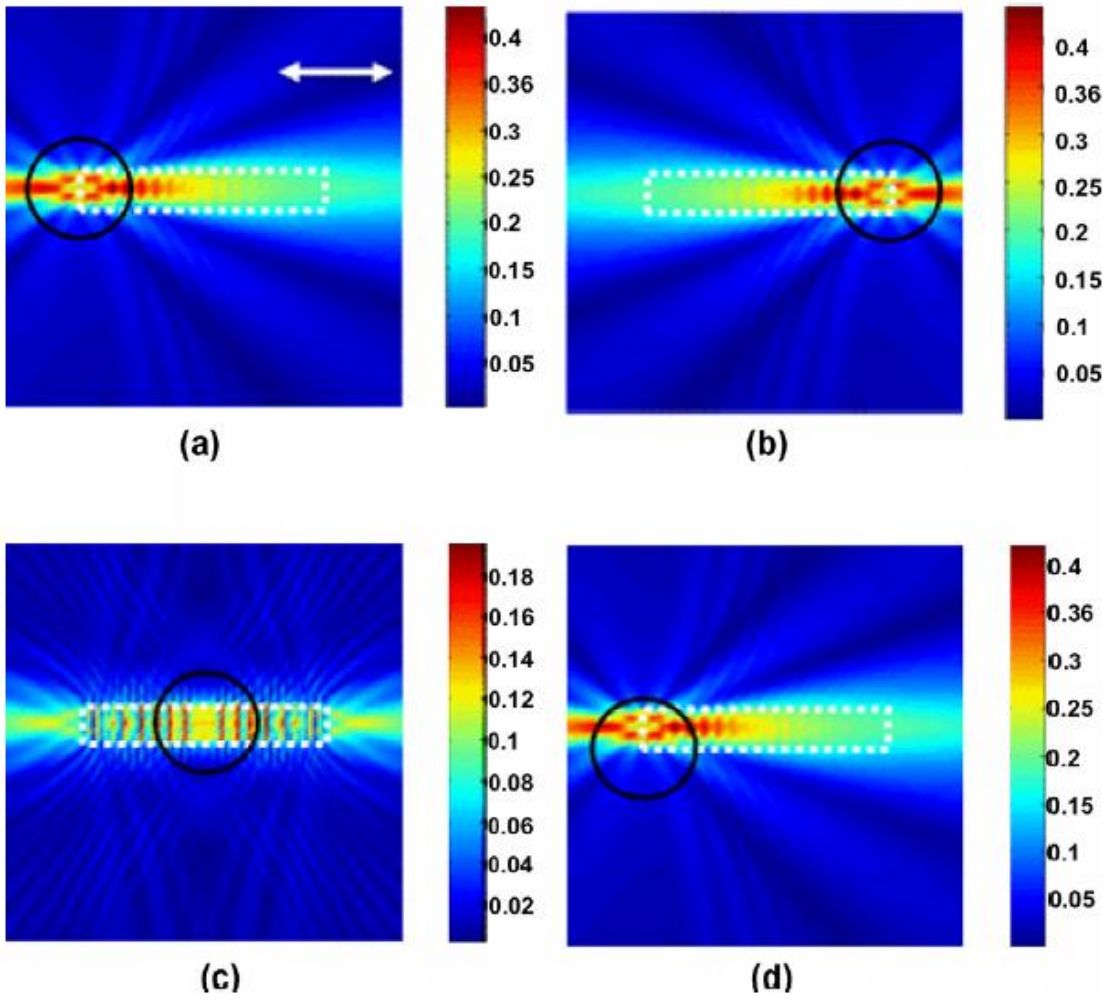

Fig. 3. Electric field magnitude distributions (20×20 μm^2) calculated for nanoarray waveguides with L=15 μm, w=2 μm, Λ=200 nm, and for incident beam positions placed at (a) left entrance (b) right entrance (c) midsection, and (d) low-corner of left entrance. The solid circle represents the incident Gaussian beam polarized along the waveguide array axis. . The arrow indicates the incident light polarization in all cases. All else is as in Figure 1(b).

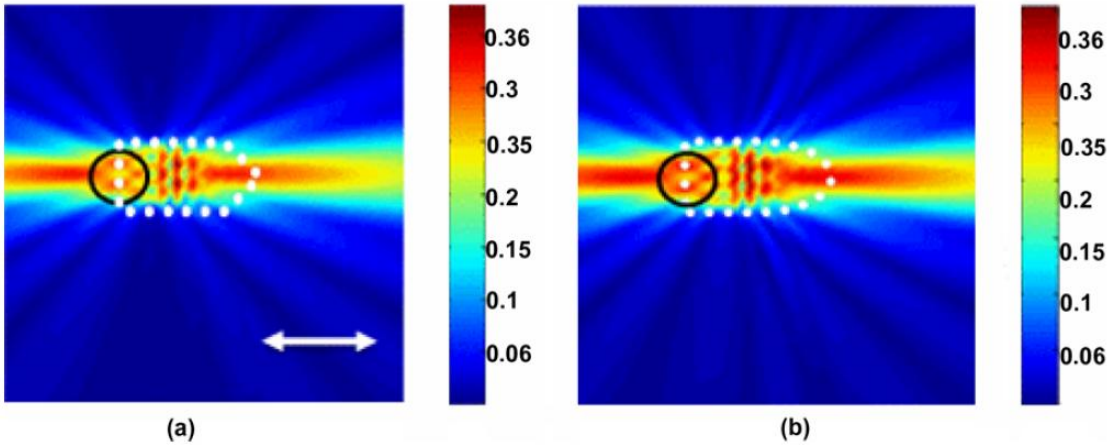

Fig. 4. Electric field magnitude distributions (20×20 μm^2) calculated for nanoarrays with tapered (a) triangular and (b) semi-circular exits shapes. The solid circle represents the incident Gaussian beam (polarized along the x-axis, FWHM=2.5 μm), L=6 μm, Λ=200 nm, and w=2μm. The arrow indicates the incident light polarization in both cases. All else is as in Figure 1(b).